Competitive adsorption within electrode slurries and impact on cell fabrication and performance

Mary K. Burdette-Trofimov*,†, Beth L. Armstrong*,‡, Luke Heroux¶, Mathieu Doucet¶, Andrés E. Márquez Rossy‡, David T. Hoelzer‡, Nihal Kanbargi†, Amit K. Naskar†, and Gabriel M. Veith*,†

†Chemical Sciences Division, Oak Ridge National Laboratory

‡ Materials Science and Technology Division, Oak Ridge National Laboratory

¶Neutron Scattering Division, Oak Ridge National Laboratory

E-mail: armstrongbl@ornl.gov, veithgm@ornl.gov

ORCID
Mary K. Burdette-Trofimov: https://orcid.org/0000-0003-2395-2867
Beth L. Armstrong: https://orcid.org/0000-0001-7149-3576
Luke Heroux: https://orcid.org/0000-0001-8993-3904
Mathieu Doucet: https://orcid.org/0000-0002-5560-6478
Nihal Kanbargi: https://orcid.org/0000-0002-7897-6957
David T. Hoelzer: https://orcid.org/0000-0001-9366-9958
Amit K. Naskar: https://orcid.org/0000-0002-1094-0325
Gabriel M. Veith: https://orcid.org/0000-0002-5186-4461

Keywords: silicon anode, polyimide, adsorption isotherms, ultra-small angle neutron scattering (USANS), slurry processing and fabrication

Abstract

Why do battery researchers use 10-20 wt% binder in research cells when commercial chemistries use much less? This report seeks to explore this question by understanding the ordering and structure of polyimide binder with a silicon/pitch-carbon black electrode system. Correlating the effect of binder concentration on electrode architecture and electrochemical properties is vital to enhancing silicon anode cycle and calendar life. Using ultra-small angle neutron scattering (USANS) and binder adsorption isotherms an optimal region of polyimide (PI) binder coverage was found. Further, there is a preferential adsorption of PI to carbon black

that has to be completed before PI binds to the silicon. Optimizing the concentration of binder leads to a 50% increase in capacity due to the optimization of binder-silicon-carbon interactions.

Introduction

A standard practice within the academic literature on silicon anodes is to prepare electrode slurries with 10-20 wt% polymer binder and 10-20 wt% carbon black, with the remainder being silicon.[1-29] Given the prevalence of this generalized electrode fabrication procedure one must wonder if this is truly the best approach to electrode fabrication and if by focusing on a generalized procedure studies may be missing key processing conditions that may result in better performing electrodes. Recently, it was demonstrated that the structure and bonding of polymers in a slurry (poly(acrylic acid), lithiated poly(acrylic acid), and short molecular weight polyimide) directly mediated the ability of silicon to reversibly cycle lithium atoms. It was found that, if the binder interacted too strongly with the silicon, lithium or electron transport during the cycling was impeded resulting in poor capacity. It was also determined that large heterogeneous domains of electroactive and inactive materials resulted in improved ion transport.[30-34] This regime was described by this group as "interzonal" where there was enough heterogeneity, i.e. discrete binder/Si/C regions versus homogeneous distribution, within the electrode to facilitate ion and electron transport while still maintaining a robust architecture to survive cycling.[30-34]

Similar to recent work showing the complexity of the binder-solids interactions, the addition of conductive carbon shows surprisingly subtle changes in concentration influence electrode performance. For example, one investigation found that adding 1 wt% reduced graphene oxide (RGO) to 14 wt% carbon black resulted in a slurry and electrode with a fully formed honeycomb-like network whereas the same electrode made with 15 wt% carbon black resulted in

the absence of a network.[35] The electrode made with 1 wt% RGO had a 24% increase in capacity at the 50th cycle when compared to the electrode without RGO, but it was not clear if the RGO addition caused the capacity increase or if it was the creation of the new, network-like structure that facilitated ion transport.[35] However, forming a network structure is highly likely as an increase in carbon-based conductive additive concentration does not result in increased capacity retention though it may affect the rate capability.[36-38] Furthermore, carbon nanotubes are also often used as both a structural component of the electrode as well as the conductive additive, but it is unclear whether the enhanced cycling of these electrodes is due to the difference in electrode architecture or the presence of a more ordered carbon.[39-43]

Various coatings, such as carbon, silica, and a variety of polymers, on silicon particles have been investigated to passivate the silicon surface.[44-53] One such coating that has received considerable attention is carbonaceous pitch.[44, 54-61] Pitch is a by-product from either the tar or petroleum industry, and generally consists of a variety of polycyclic aromatic hydrocarbons.[62-64] Pitch has been shown to mitigate the volume expansion and pulverization of silicon upon cycling and helps create a more stable secondary electrolyte interphase (SEI), resulting in reduced capacity fade.[65] One investigation of pitch coated silicon observed that a 2.5 fold increase in pitch content resulted in an increase in capacity retention by 27% in a half cell on the 200th cycle.[65] The pitch coating was made by electrospraying a dispersion of silicon and pitch. This investigation claimed that the differences seen in the electrochemical properties were due to the higher pitch content preventing pulverization.[65] A second study that used pitch coated silicon found that increasing the Si content (up to ~15 wt%), thus reducing the pitch concentration, increased the reversible capacity of the electrode, in a half cell, by 33%.[66] Finally, pitch is a low cost carbon product that may be

compatible with the economics of Si electrodes and is under investigation by the US Department of Energy's Silicon Consortium Project.

This work focuses on the role of PI binder concentrations on slurry dynamics and the resulting electrode performance for silicon electrodes, encapsulated with carbon pitch. The results show distinct regions of molecular interactions which drive electrode performance and identify a generalized approach to optimize electrode chemistry through binder adsorption isotherms.

Experimental

Reagents and Solvents

All reagents were used without further purification. The polyimide binder, P84, was obtained from Ensinger (Austria) and was received as a solid, yellow powder. Petroleum Pitch ZL 250M (hereafter referred to as pitch) was obtained from Rain Carbon Inc. (Germany). Silicon boules (El-CAT) were cleaned sequentially in hot acetone, methanol, a 5:1:1 (volume) mixture of DI water, NH_4OH (Fisher – Reagent Grade); H_2O_2 (Fisher – Reagent Grade 30%), and < 1 minute dip in a 5 wt% HF solution. *Care should be taken with this procedure due to the exothermic nature of the H_2O_2 treatment and the toxicity of HF.* C-NERGY Super C45 conductive carbon black (C45) was purchased from Timcal. Deuterated DMF-D7 (D, 99.5%) was purchased from Cambridge Isotope Laboratories, Inc. (Tewksbury, MA). DMF for electrode fabrication was purchased from Sigma Aldrich (ACS reagent, ≥ 99.8%). Deuterated dimethylformamide (DMF) is similar in polarity and functionality when compared to NMP, where DMF-D7 is availability in quantities required for this work while deuterated NMP is not.

Si@pitch Powder Synthesis

Silicon boules (100g, 1-3 cm in length) were milled using a Zoz Simoloyer CM01 high energy ball mill (Wenden, Germany) charged with 1000 g of 5 mm spherical 440C stainless steel milling media (Union Process). The jacket of the milling chamber was cooled with a recirculating chiller equipped with an ethylene glycol/water mixture that was cooled to 15°C. The mill was cooled for at least 1 hour prior to the start of the mill run. After loading the mill with silicon boules, the mill was evacuated using vacuum and refilled with argon. This cycle was repeated 3 times resulting in a milling atmosphere of argon prior to the milling process. The silicon boules were milled for 90 minutes at 700 rpm. The subsequent silicon powder was collected in an argon filled jar, which was placed in an argon-filled glovebox after collection. This Zoz milled silicon powder was used in the next milling process.

The Zoz milled silicon powder and pitch were milled together using a Retsch CryoMill (Haan, Germany) cooled with liquid nitrogen. For the Si@pitch material with a ratio of 90:10 or 50:50 Si:pitch, the CryoMill jar was loaded with 10 g Si and 1.125 g pitch or 5 g Si and 5 g pitch, respectively, in an argon glovebox. The milling process consisted of a pre-cycle at a frequency of 5 Hz for 5 minutes followed by a milling cycle at 30 Hz for 40 minutes. This procedure was repeated 6 times after which the Si@pitch powder was collected, Figure S1 (top). Both the 90:10 and 50:50 Si@pitch cryomilled powders were annealed in a tube furnace with flowing argon for 1 hour at 700°C using a ramp rate of 5°C/min. During this thermal annealing process, the pitch is pyrolyzed to its carbon derivatives. Prior to the annealing process, the quartz tube—with the sample inside—was purged with argon for 1 hour. The annealed powder was placed in the CryoMill jar in an argon environment and was cryomilled using a 5 Hz, 3-minute pre-cycle followed by one 30 Hz, 15-minute cycle. These powders were used to make slurries for electrodes and neutron scattering experiments.

Slurry Preparation Method

To prepare 10 wt% solutions of PI binders, P84 was placed in DMF-D7 or NMP (~25 mL) and was mixed using a Thinky brand planetary centrifugal mixer (PCM) at 2000 rpm for two-2 min intervals until the P84 powder was fully dissolved. Each Thinky brand mixing jar had 5 pieces of 5 mm yttria stabilized zirconia (8 mol%) (8YZ) media.

To prepared Si@pitch slurries for rheological and electrochemical analysis, the slurry was made in the following order and mixed with the PCM: 1) NMP and P84 (0.5 wt% used as a dispersant) were mixed for 30 seconds at 2000 rpm, 2) Si@pitch 90:10 or 50:50 were added to the slurry and mixed one time at 2000 rpm for 2 min, 3) C45 was added to the slurry and mixed twice at 2000 rpm for 2 minutes, 4) P84 (10 wt% in NMP) solution was added to the slurry and mixed once at 2000 rpm for 2 minutes. See Table 1 for the composition of each slurry prepared. Si@pitch 90:10 and 50:50 slurries for neutron scattering experiments were fabricated using the PCM and were mixed using the same protocol as described above, omitting the C45 step, as there is no carbon black in the slurries for neutron scattering.

Table 1: Amounts of each constituent in each electrode for a given electrode formulation.

Electrode Formulation	Amount of Si@pitch (90:10 or 50:50 ratio)	Amount of C45	Amount of dispersant P84 10 wt% solution	Amount of binder P84 10 wt% solution	Amount of extra D-DMF or NMP
Si@pitch:C45:P84 80:10:10	2 g	0.25 g	0.13 g	2.38 g	3.00 g
Si@pitch:C45:P84 90:5:5	2 g	0.11 g	0.11 g	1.00 g	2.25 g
Si@pitch:C45:P84 88:2:10	2 g	0.045 g	0.12 g	2.16 g	1.94 g
Si@pitch:P84 90:10	9 g	--------	0.50 g	9.50 g	12.25 g
Si@pitch:P84 95:5	9 g	--------	0.53 g	4.77 g	15.50 g

Si@pitch:P84 99.5:0.5	9 g	--------	--------	0.45 g	18.80 g

Gel Permeation Chromatography

Molecular weight of the P84 binder was determined using gel permeation chromatography (GPC) using an Agilent 1100 series Autosampler (1313A), quaternary pump, vacuum degasser, column oven (Waters Temperature Control Module II), and a flow-cell refractive index detector (ERC RefractoMax520). Both the columns and the refractive index detector were heated to 35°C. A Jordi polystyrene mixed bed column with a molecular range of 500 g/mol to 2 million g/mol, and a Jordi guard column were used.

P84 was dissolved in HPLC grade NMP (5 g/mL, Sigma Aldrich). The sample equilibrated for a minimum of 24 hours prior to filtration and injection. The solution was filtered through a 0.2 µm PTFE syringe filter prior to injection (40 µL) where the eluent was HPLC grade NMP. Flow rate was 0.75 mL/min. Chromatograms were analyzed with Agilent ChemStation software. The measured weight average molecular weight (M_w) of P84 is 24,539 g/mol with a PDI= 10.47.

Binder Adsorption Isotherms

Binder adsorption isotherms were measured through refractive index on a Mettler Toledo RM40 Refractometer. Twelve dilute (0.25 wt% to 10 wt%) solutions of P84 in NMP were measured using the refractometer to make a calibration curve. A series of C45, Si@pitch 90:10, or 50:50 (0.5 g) slurries containing 0.25 wt% to 10 wt% of P84 (with respect to C45 or Si@pitch) were fabricated. These slurries were shaken on a rocker table for 1 week in a dark box to ensure maximum adsorption. The slurries were subsequently centrifuged at 6000 rpm for 1 hour and the supernatant was removed, and its refractive index was measured. A competitive adsorption study

between C45 and silicon powder (no pitch) was performed by mixing silicon (2 g) with 1 wt% of P84. This slurry was mixed on the rocker table for 1.5 weeks. Then C45 (5 wt% with respect to silicon) was mixed into the slurry for 0, 5, 10, 20, 30, 40, 50, or 60 minutes. Each slurry was centrifuged at 6000 rpm for 20 minutes after each time slot. The refractive index of the supernatant was measured for each slurry.

Brunauer–Emmet–Teller (BET) Surface Area Analysis

Nitrogen adsorption and desorption experiments were run on Quantachrome Autosorb iQ at 77 K. The Brunauer–Emmet–Teller (BET) model of isotherms was utilized, and the adsorption of N_2 at small relative pressures was fit to calculate surface areas of each sample.[67] In a typical experiment, ~150 mg of sample was loaded into a 9.0 mm cell. Degassing was performed by heating the sample at a rate of 2°C/min to a maximum temperature of 300°C for a period of 12 hours. Once the degassing step was complete, the cell volume was replaced with helium and weighed again. The sample was then analyzed in the BET using a P/P_0 range of 0.0002 to 0.99.

Neutron Scattering

Neutron scattering measurements were obtained at the Spallation Neutron Source (SNS) at Oak Ridge National Laboratory (ORNL) using the USANS instrument (BL-1A). Rheology coupled ultra-small angle neutron scattering (rheo-USANS) to probe slurry structure from 200 nm to 10 μm. For all USANS measurements, the neutron scattering intensity is measured as a function of Q, the neutron wave vector transfer as shown by Equation 1, where θ is the scattering angle, and λ represents the neutron wavelength.[68] The USANS instrument at SNS is a time-of-flight triple-bounce Bonse-Hart small-angle scattering instrument where measurements are obtained from Q= 0.0001 to 10^{-5} $Å^{-1}$.[69, 70] All neutron scattering measurements were collected using the 3.6

and 1.8 Å reflection of the analyzer crystals. Raw data were reduced using the Mantid framework to calculate I(Q).[71] A background measurement was performed with the empty concentric cylinder geometry using identical sampling conditions. The background measurement was subtracted from the sample measurement. Neutron data were modeled using the SasView small-angle scattering software package.[72] USANS data were not normalized, and the overall normalization was fitted along with the other model parameters when modeling I(Q).

$$Q = \frac{4\pi}{\lambda}\sin\left(\frac{\theta}{2}\right) \qquad \text{Eqn (1)}$$

The rheometer on the USANS beamline is an Anton Paar (Ashland, Virginia) Physica MCR501. The geometry used was a concentric cylinder with a 49 mm quartz bob and a 50 mm quartz cup. A solvent trap was used to abate solvent evaporation. Each rheo-USANS measurement was performed at a constant shear rate of 0, 30, 200, or 500 Hz where 200 and 500 Hz represent typical shear rates used for slot die-like coaters. In contrast, hand-cast electrodes tend to be cast in the 61 to 1200 Hz range where the gap is 25-500 μm. The 30 Hz and 0 Hz shear rates correlate to the slurry being fed from the hopper to the slot die and at rest, respectively.

Electrochemical Testing

A 1 mil (25 μm) doctor blade was employed to cast the Si@pitch slurries onto copper foil (battery grade) where the approximate shear rate was 610 Hz—calculated using the simple shear rate equation.[73] The cast electrodes were dried on a hot plate at 120°C in air; then they were annealed at 245°C under dynamic vacuum (-28 in. Hg) for 2 hours. This 245° annealing is hypothesized to introduce porosity essential for electrolyte infiltration. After cooling, electrode disks (14 mm) were punched with a high precision EL-Cut electrode cutter obtained from EL-Cell (Hamburg, Germany). After curing electrode disks were dried at 120°C in the vacuum oven (28 in

Hg) for approximately 18 hours. The electrode disks were transferred to an argon filled glovebox while still hot to prevent moisture contamination. The active loading of Si@pitch was approximately 0.1-0.2 mg/cm^2, and the electrodes were not calendared after fabrication. This low loading was selected to overcome tortuosity limitations of small silicon particle electrodes which limit performance in thicker materials. Coin cells (2032 type – Pred Materials, NY) were assembled in an argon glovebox in the following order: coin cell cap, gasket, wave washer, spacer with lithium metal adhered, one 18 mm disk of Dreamweaver Gold separator, 100 μL of 1.2 M lithium hexafluorophosphate solution in battery grade ethylene carbonate and ethyl methyl carbonate (50/50 (v/v)) (Aldrich – UBE Chemical) electrolyte, Si@pitch anode, coin cell bottom. Each half cell was cycled at C/5 between 1 V and 50 mV using a MACCOR battery test stand at 30°C. This limited window is designed to limit SEI dissolution. Prior to discharge, the half-cell rested for 10 minutes. Between the discharge and charge step, the half-cell rested for 10 minutes.

Results and Discussion

This work focuses on correlating the binder-silicon interactions as a function of processing conditions (weight percentage, materials chemistry). The interactions are extracted from adsorption isotherms and neutron scattering since direct measurements with electron microscopy are impossible *ex* and *in situ* due to the contrast between the solvent and polymer, incompatibility of the microscopes with NMP, and difficulty imaging sub-monolayer coatings and structures of polymers on a carbon coated silicon.

The silicon active material used in this investigation taken from silicon boules from the semiconductor industry that have been milled into a powder with a median particle size (D50) of sub-10 μm. Representative scanning electron micrographs (SEMs) are shown in Supporting

Information, Figure S1. Once the silicon powder is obtained, it is milled at liquid nitrogen temperatures (i.e., cryomilled) with a petroleum-based pitch comprised of various polyaromatic hydrocarbons. The mill must be kept cold to prevent the pitch from melting and making large, fused Si@pitch aggregates.

As noted in the introduction it is hypothesized that varying the concentration of binder and carbon in a slurry affects electrode structure, processing, and performance. To test this hypothesis, binder adsorption studies were performed to identify regions of interest for more detailed studies of the polymer-anode interactions. Two distinct carbon pitch coating concentrations were chosen to reflect different surface compositions and their effect on the adsorption of PI.

To measure the binder adsorption properties as a function of binder content, refractive index (RI) data were collected. RI measurements are highly sensitive to changes in the chemical environment in a solution.[74-76] Figure 1 presents the refractive index-derived adsorption isotherms plotted as wt% of PI in the supernatant of the slurry versus wt% of the PI originally added to the slurry. Raw data are shown in Figure S2. Each refractive index point in Figure 1 is the average of 3 points where each measurement had a maximum difference of 0.0001 (unitless). An error of 0.0001 would account for an error of 0.05% of the weight percent polyimide in solution. A control experiment utilizing 10 wt% P84 that was centrifuged revealed that only 0.05% (of the 10% - one RI Unit) was removed through centrifuging. This represents a maximum potential removal of P84 from the supernatant though, when combined with the powders, will be much lower after absorption of the removable P84 through adsorption and is not a significant source of error in these measurements.

Analysis of this data reveals three apparent adsorption zones for the two Si@pitch materials as evident by the change in slope with changing concentration. First, there is a tightly bound layer

(< 1 wt%) as evident by there being no residual PI in solution. Second, a region between 1 and 5 wt%. Then a third region at higher concentrations (>5 wt%). Note, the surface does not appear to reach saturation as evident by the continued removal of PI from solution through adsorption on the silicon. This type of adsorption isotherm is classified as a Freundlich isotherm in that the adsorption sites are non-specific, and the surface does not become fully saturated.[77] In essence, the Si-pitch surface is heterogenous with varying adsorption affinities. These adsorption sites are dynamic, meaning adsorption and desorption of PI are likely to occur simultaneously and/or have some dimensionality, i.e., are multilayered. This is in contrast with Langmuir adsorption isotherms which assumes that the PI is adsorbed as a monolayer onto the Si-pitch surface and is fully adsorbed when the surface is completely covered by the binder. Langmuir also assumes that this occurs with limited, site specific adsorption.[77] Strong interactions between the PI and silicon surface are dominant at low concentrations, and is followed by more dynamic interactions with increasing binder content. These dynamic interactions are indicative of diffusive interactions due to polymer-polymer attractive forces, which dominant over silicon-polymer interfacial forces.

From BET, Figure S3, the measured surface area of Si@pitch 90:10 and 50:50 were 44 m^2/g and 148 m^2/g, respectively. From the density of the PI and BET surface areas of the Si@pitch materials, assuming a perfectly homogeneous coating, at binder concentrations < 1wt%, would lead to a PI coating on the Si@pitch 90:10 and Si@pitch 50:50 between 0.09 and 0.05 nm thick, respectively. These thicknesses are not likely, because the PI is larger than the size of 2-3 carbon-carbon bonds and point to the selective adsorption of discrete polymer clusters or aggregates as schematically represented in Schematic 1 (dark blue circles). The Si@pitch 50:50 powder can fully adsorb 1 wt% PI binder because the surface area of Si@pitch 50:50 is 3.5 times larger than the Si@pitch 90:10 material, which results in an overall thinner layer (by about 2x) of tightly bound

P84 on the surface of the Si@pitch 50:50 powder. Assuming a larger thickness, the Si@pitch 90:10 powder would have more bare areas than the 50:50 powder, resulting in a more "blotchy" P84 coating. While it is possible for the tightly bound layer to change under electrode processing (i.e., flow) conditions, it is more likely that this layer is the least dynamic as discussed subsequently in the USANS data.

When the P84 concentration is increased, there is a dramatic change in the adsorption behavior where less than half of the available P84 is bound to the surface for each Si@pitch powder although the Si@pitch 50:50 powder adsorbs more P84 at all concentrations (Figure 1). The second layer on the Si@pitch materials is imagined as a loosely bound P84 layer, which is represented by the blue spirals in Schematic 1. This layer is either adsorbed onto Si@pitch directly or interacts with the fully adsorbed layer where part of the P84 chain extends into the solvent phase. As with the other two layers, the diffuse layer on the Si@pitch 50:50 powder is thinner than the one on the Si@pitch 90:10 powder. This is the most dynamic layer on the Si@pitch powder as detailed in the USANS data analysis section. The adsorption or lack thereof of the binder to the active material is one of the critical roles of the binder in the electrode i.e., to hold the silicon together during cycling. If the majority of the binder is not participating it potentially adds unnecessary complexity and side reactions. In addition, the organization of the binder will also impact the structure of the resulting electrode after processing.[34] Thus, understanding how the adsorption and diffusion on the P84 changes under processing conditions is key in improving electrode fabrication and electrode chemical behavior as well.

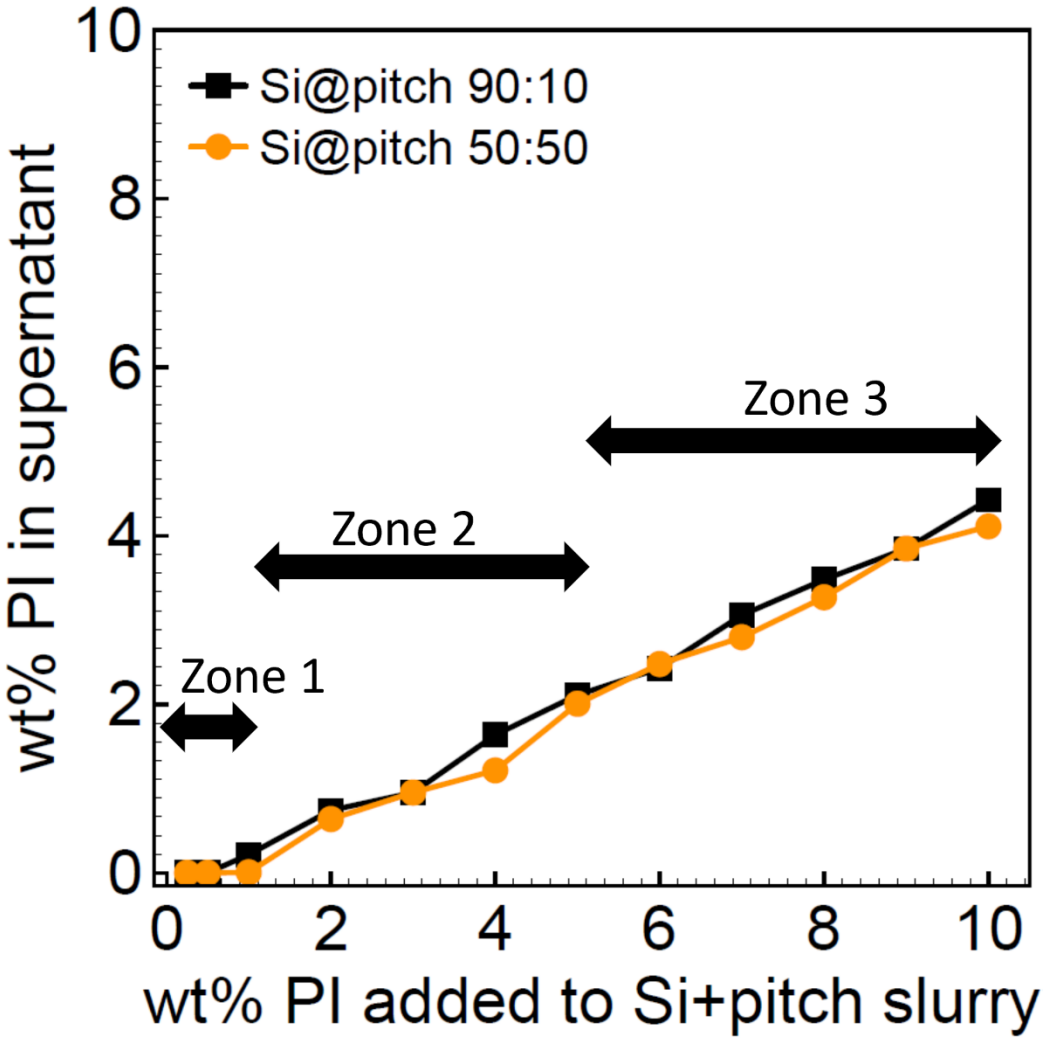

Figure 1: Amount of P84 (wt%) in the supernatant of Si@pitch 90:10 (black squares) and 50:50 (orange circles) as a function of total amount of P84 added to the Si@pitch slurry. The amount of P84 in the supernatant is directly measured from the refractive index of the supernatant of the slurry. Each adsorption isotherm is highlighted by the shaded area.

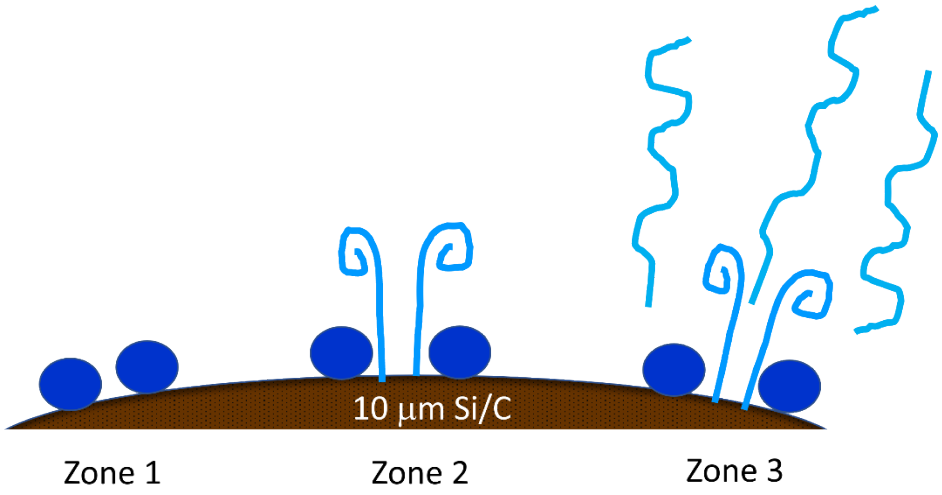

Schematic 1: Pictorial depiction of the density and thickness of the tightly bound layer (dark blue spheres), the loosely bound layer (blue spirals), and the diffuse layer (light blue lines) on Si@pitch powders as determined by refractive index measurements, density of P84, and BET surface area and USANS data. Top left shows representative electrode surface after drying.

Typically, a silicon anode is not composed solely of silicon but is a composite material, which also contains carbon black. When both silicon and carbon black are present in the slurry, the binder may preferentially adsorb onto one surface or another resulting in competitive adsorption of P84. To fully understand the behavior of the P84 binder in the electrode slurry, the P84 adsorption onto carbon black (C45) must also be elucidated. Completely the same refractive index study as presented for Si@pitch, Figure 2A, shows that C45 adsorbs nearly all of the binder up to 9.5 wt% P84. This adsorption data would indicate in a 10 wt% binder slurry most of the binder segregates to the carbon black.

To evaluate the competitive adsorption of P84, P84 (1 wt%) and silicon (without pitch) were mixed. Then C45 was added to the slurry and the RI of the supernatant was measured at different times after the C45 addition. From Figure 2B, there is an immediate adsorption of P84, which is likely due to available P84 adsorbing onto C45 since silicon powder can only adsorb approximately 0.5 wt% P84.[30] It is interesting to note that the immediate adsorption at time=0 is

not 100%. It is hypothesized that this is due to the kinetic effects of adsorption or within the error of the measurement as discussed above. As the slurry "ages" from 5-40 minutes, there is an apparent (small) increase of P84 in the supernatant consistent with a change in RI of ±0.0001. This could be due to P84 desorbing from silicon and not yet having time to adsorb onto the C45 or reflects the limit of the measurement. A data point measured after 3 days revealed about 0.4 wt% PI unbound consistent with a complex equilibrium. Regardless, the change in adsorption behavior over time indicates that the binder interactions with the slurry solids is dynamic, and likely plays a role in electrode properties depending on the time in solution before casting into the electrodes.

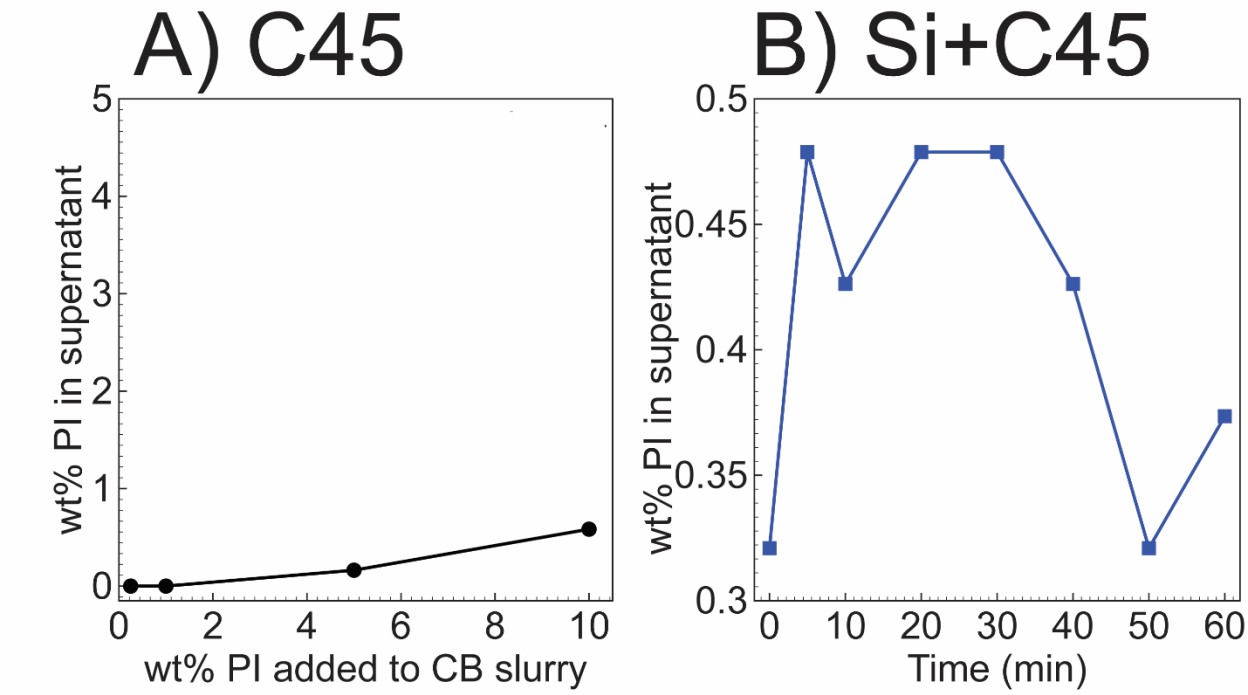

Figure 2: A) Amount of P84 (wt%) in the supernatant, as measured by RI, of C45 slurries (black squares) as a function of total amount of P84 added to the slurry. B) Amount of P84 in supernatant of Si+C45 slurry, as measured with RI, plotted as a function of time after C45 addition.

Structure and Flow Behavior of Si@pitch Slurries with Different Pitch Ratios

From the binder adsorption isotherms shown in Figure 1, there are 3 approximate P84 adsorption regimes. To evaluate the binder/silicon structure of the slurries in the various

concentration regimes, Si@pitch slurries were prepared with 0.5 wt%, 5 wt%, and 10 wt% P84 for ultra-small angle neutron scattering (USANS) studies (Figure S4). Carbon black was not introduced in the USANS slurries as the scattering from carbon black cannot be contrast matched and instead would overwhelm the signal from the binder, therefore we focus only on the Si@pitch-PI interactions. Figures 3 and 4 present representations of the agglomerate and aggregate structure of Si@pitch 90:10 and 50:50 slurries with varying amounts of P84 binder as extracted from fitting of the USANS data from the correlation length model (CLM) described by Equation 2 (See Supporting Information for fits and values).

$$I(Q) = \frac{A}{Q^n} + \frac{C}{1 + (QL)^m} + B \qquad \text{Eqn (2)}$$

The CLM uses five parameters: A, C, L, n, and m.[78, 79] The A parameter describes the agglomerate structures that are 2-10 μm in size though the A parameter has an inverse relationship with size, meaning a smaller A value describes a larger agglomerate structure. Parameter C characterizes the number and size of aggregates, which are structures 500 nm to 1 μm in size. Aggregates are comprised of smaller units called clusters whose size is described by the correlation length parameter, L. The n and m parameters describe the shape or smoothness of the aggregates and the density of polymer chain or aggregate packing, respectively.[31, 32] In the Figures 3 and 4, the agglomerate structure is represented by the amount of overlap of each ellipsoid and the aggregate structure is represented by the number and size of each differently colored ellipsoid. All structures are interpreted based on the USANS scattering curves (shown in Supporting Information).

From Figures 3 and 4, it is immediately noticeable that the amount of pitch on the silicon surface has an impact on the structure of the slurry. All Si@pitch 50:50 slurries have fewer and

smaller agglomerates than the Si@pitch 90:10 slurries except for the slurries with 5 wt% P84 at 30 Hz and 200 Hz and 0.5 wt% P84 at 0 Hz. The density of aggregate (m parameter) and shape of the aggregate (n parameter) do not have a large influence on the overall structure and behavior of the slurry as there are no clear trends in the data. For a more in depth look into the individual parameters and how they change with shear rate, see Supporting Information.

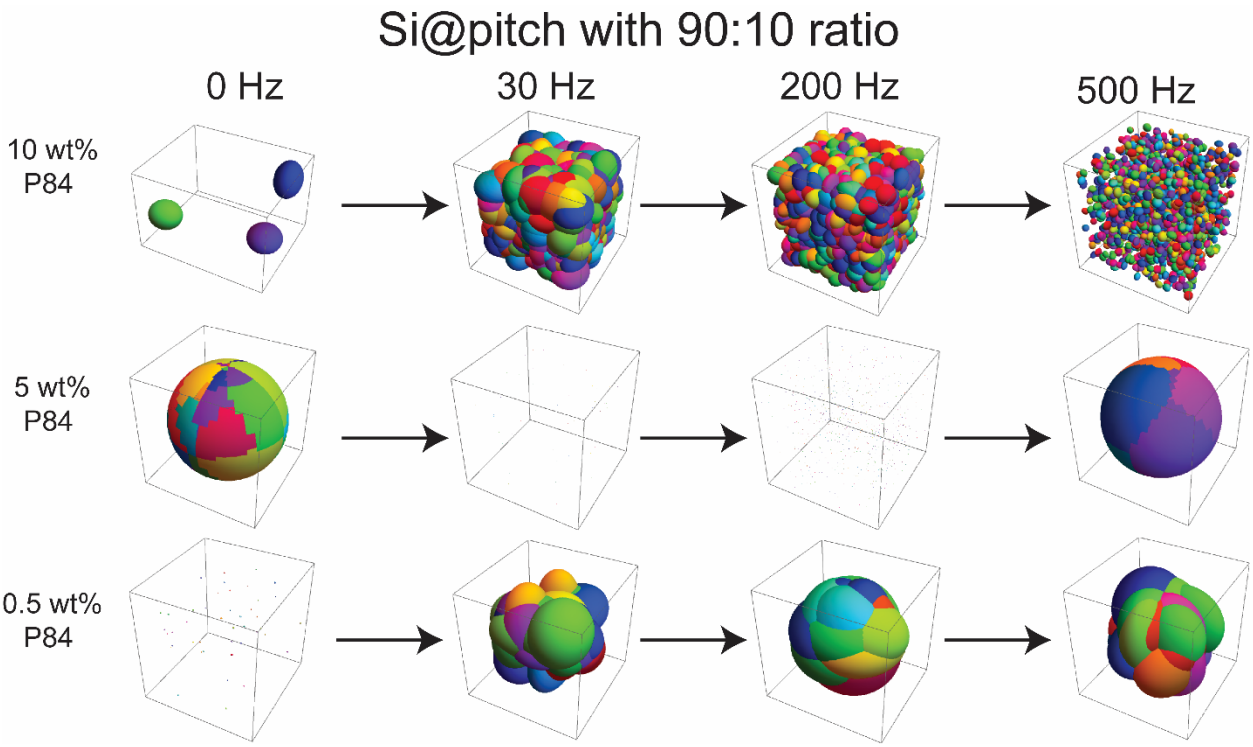

Figure 3: Schematic representation of Si@pitch 90:10 slurries with P84 concentrations of 10 wt% (top), 5 wt% (middle), and 0.5 wt% (bottom). Each slurry was sheared at 4 different shear rates: 0, 30, 200, and 500 Hz. Each differently colored ellipsoid represents the size and shape of the aggregate while the extent of overlap of each ellipsoid represents the number and size of agglomerates. The boxes that appear empty, namely the 5 wt% P84 at 30 and 200 Hz, and the 0.5 wt% P84 at 0 Hz, are comprised of very small (~200 nm) aggregate and agglomerate species.

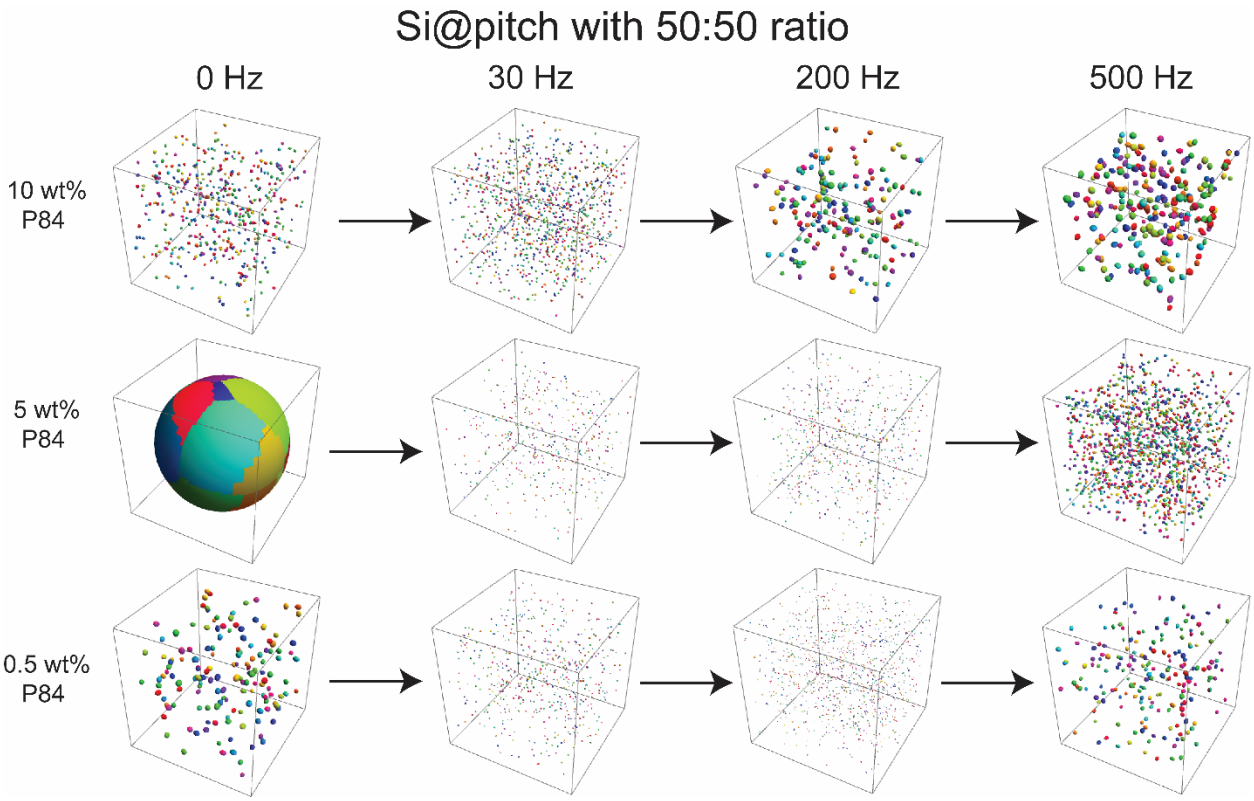

Figure 4: Schematic representation of Si@pitch 50:50 slurries with P84 concentrations of 10 wt% (top), 5 wt% (middle), and 0.5 wt% (bottom). Each slurry was sheared at 4 different shear rates: 0, 30, 200, and 500 Hz. See Figure 4 for details on interpreting the schematic.

Si@pitch 90:10 slurries

From the USANS data, at 0 Hz, there are 3 vastly different binder-silicon structures depending on the binder concentrations. This data also shows the distinct impact of adsorption regimes evident in the adsorption isotherms. The Si@pitch 90:10 with 0.5 wt% P84 has the fewest number of agglomerates by 8 orders of magnitude. The overall shape of the aggregates for the Si@pitch 90:10 slurry with 0.5 wt% P84 are the most linear (n=1.43) resulting in the largest correlation length at 539 nm, i.e., has the largest primary cluster size. The behavior is most likely due to the 0.5 wt% P84 acting as a dispersant,[30] a small molecule or low molecular weight polymer that adsorbs onto particles sterically stabilizing them in the slurry, since the M_w of P84 is in the molecular weight range of a dispersant.[80-83] The refractive index data also shows that 0.5 wt% P84 on the Si@pitch 90:10 is fully adsorbed, so there is little interaction among the Si@pitch 90:10

particles in suspension. With shear, the particles aggregate extensively indicating the possible elongation of and/or interaction between bound polymer units.

At 0 Hz, when P84 concentration is increased to 5 wt%, the most agglomerated and aggregated structures—by at least an order of magnitude—are created. At 5 wt% P84, approximately 2.5 wt% P84 is not adsorbed to the Si@pitch material as shown with the RI data, so the severe agglomeration and aggregation occurring in this slurry is likely due to 1) the loosely bound or diffuse layer of P84 interacts with more than one particle[84], 2) the "free" P84 entangles with the loosely bound layer, and 3) or a combination of the two. Upon an increase in shear rate, the entanglements are cleaved, leaving a much more dispersed system until 500 Hz where there may be enough shear force to cause re-agglomeration.

When the concentration of P84 is increased to 10 wt% the structure of the slurry is highly dynamic under the varying flow conditions likely due to the diffusion/adsorption behavior of the diffuse layer shown in the RI data. From the adsorption isotherm data, it was shown that only 0.5 wt% P84 is directly adsorbed on the Si@pitch surface. Thus, 9.5 wt% of P84, in essence, is acting as a secondary discrete material in the slurry, which can result in separate agglomerate interactions. So as the shear rate increases from 0 Hz to 30 and 200 Hz, the 10 wt% P84 slurry has an increase in the number of agglomerates by at least an order of magnitude where the agglomerates can be composed of silicon-silicon, silicon-P84, or P84-P84. The high concentration of P84 and the presence of the diffuse layer results in the particles being "tied" together. This type of behavior is often seen when a dispersant-like molecule is used in too high of a concentration.[85]

Drawing an image of the Si@pitch surface in the slurry would be composed of a tightly bound polymeric layer and a second layer of loosely bound P84, and, lastly, a diffuse layer composed of fully solvated P84. Both the adsorption isotherms and USANS data indicate that there

is an optimum concentration,[30] where concentration of the binder promotes dispersion or enhances entanglement of the binder (and encapsulation of the silicon in an insulating/ion blocking layer). From the USANS data alone, it would seem that the 5 wt% P84 slurry, when cast between 30 and 200 Hz, would result in the most uniform and homogenously dispersed silicon within the electrode. From previous work, it was found that a slightly agglomerated, but dispersed, electrode architecture resulted in cells that cycled while a slurry that consisted of well dispersed particles did not cycle as well.[31, 33] It was hypothesized that this was due to porosity providing a network for lithium-ion diffusion, but a network of interconnected active material.[86] Furthermore, a slurry that was highly agglomerated, and not well dispersed, also resulted in cells that cycled poorly.[30] It stands to reason then that the 0.5 wt% P84 silicon slurry (i.e., no carbon black) would result in the electrode with the best electrochemical properties because it has the intermediate agglomerate structure from 30-500 Hz. However, with carbon black present in the electrode slurry, it is likely that all of the 0.5 wt% P84 would adsorb onto the C45, leaving the Si@pitch material bare and the electrode would not have enough structural integrity to support lithiation/delithiation. Following this logic, if 10 wt% C45 is added to the electrode slurry, 9.5 wt% P84 adsorbs onto the carbon black and 0.5 wt% will adsorb to the Si@pitch powder creating a slurry morphology similar to the one depicted in the 0.5 wt% P84 USANS data. This electrode may support extended electrode cycling.

Si@pitch 50:50 slurries

At 0 Hz, the structure of the Si@pitch 50:50 slurries at all concentrations of P84 is similar to that of their Si@pitch 90:10 counterparts. When shear is increased to 30 Hz, all slurries experience a decrease in agglomeration while maintaining a similar number of aggregates. In this case, it appears that the shear rate is cleaving the agglomerates from each other in all slurries. This

is the opposite behavior as to what was observed in the Si@pitch 90:10 slurries containing 0.5 wt% and 10 wt% P84. Decreasing the number and size of agglomerates is typical when shear is applied to a slurry as the shear force breaks the agglomerates,[87] but the opposite behavior is observed in the Si@pitch 90:10 slurries. This points to a difference in adsorption/diffusion behavior of the loosely bound and diffuse layer on P84 for the different Si@pitch powders. This may indicate the P84 layers on Si@pitch 90:10 extend further into the solvent phase, increasing the shear rate causes the extended P84 chains to entangle with one another, creating an interconnected network of P84/Si@pitch. Conversely, the P84 chains on the Si@pitch 50:50 are more closely packed together, so, upon shearing they do not entangle as much with other P84 chains, but rather stay as discrete particles. This is likely why shear does not have a great effect on the overall structure of the Si@pitch 50:50 slurries. At 200 and 500 Hz, the 5 wt% and 0.5 wt% are the most dispersed, least agglomerated systems (by at least 2x). At 200 Hz and 500 Hz, an electrode cast from Si@pitch 50:50 with 5 wt% or 0.5 wt% P84 would be the most homogeneous electrodes—perhaps too homogeneous— though it is unlikely that 0.5 wt% P84 is enough binder to provide mechanical strength to the electrode film.

Electrochemical Analysis

To explore the effect of pitch, P84, and C45 concentration electrodes with Si@pitch 90:10 and Si@pitch 50:50 active materials 3 sets of electrodes were made with Si@pitch:C45:P84 formations of 80:10:10, 90:5:5, or 88:2:10. A representative image of the electrode is shown in Figure S5 and reveals a dense electrode surface with no significant porosity. Specific capacities as a function of cycle are in Tables S9-11. The 80:10:10 electrode was chosen as it represents the 0.5 wt% P84 USANS slurry where 9.5 wt% P84 adsorbs onto C45 and 0.5 wt% adsorbs onto Si@pitch 90:10. The 88:2:10 slurry represents the 10 wt% P84 USANS slurry in that there is

excess P84 available to adsorb onto silicon. This electrode is also representative of the binder adsorption isotherm data with all 3 layers (of P84 on the Si@pitch 90:10. The 90:5:5 electrode represents the 5 wt% P84 where there is a sub-optimal amount of P84 present in the solution to cover both the C45 and the Si@pitch 90:10. The same electrodes were fabricated with the Si@pitch 50:50 as the active material to show the effect of intentionally dosing the material with less-than-ideal P84 binder ratios.

From Figure 5, which shows the voltage versus specific capacity profile of each electrode, the Si@pitch 90:10 electrode with 10 wt% C45 and 10 wt% P84 outperforms all other electrodes—with a capacity approaching theoretical limits (3600 mAh/g Si). From the binder adsorption data and the rheo-USANS data, this is likely because the optimal ratio of P84 to Si@pitch and C45 has been obtained where 9.5 wt% binds to C45 and 0.5 wt% binds to Si leading to an optimal binding configuration. In the Si@pitch 90:10 electrode with 5 wt% C45 and 5 wt% P84, it is likely that almost all of the P84 is binding to the C45, leaving little P84 available to Si@pitch, which causes the cycling of the electrode to suffer. Furthermore, when a Si@pitch 90:10 electrodes was made with 10 wt% C45 and 0.5 wt% P84, the electrode would not cycle at all likely because there is no strength to the electrode.

When the C45 content is reduced to a more industrially relevant concentration—2 wt%—the capacity on the first cycle of the Si@pitch 90:10 electrode is reduced by approximately 25% (Figure 5c) when compared to the 80:10:10 electrode (Figure 5a). Since the 2 wt% C45 is only able to adsorb a maximum of 2 wt% P84, there is an excess of P84 around the Si@pitch powder making lithium-ion diffusion difficult as shown by the intense agglomeration and aggregation behavior shown via rheo-USANS of the Si@pitch 90:10 material with 10 wt% P84.

From Figure 5, the Si@pitch 50:50 electrodes have a noticeable lower capacity than their Si@pitch 90:10 electrode counterparts due to the 44% lower active Si material. Accounting for this difference in Si material the capacity of the 50:50 materials is roughly 30 to 50% lower than the analogous 90:10 samples pointing the P84 to C45 ratio not being optimized (90/5/5 and 80/10/10 ratio respectively). Since the surface area of the Si@pitch 50:50 material is over 3 times greater than the 90:10 material, the Si@pitch 50:50 powder can adsorb more P84 (up to 1 wt%) as shown with the refractive index measurements. Therefore, having 9.5 wt% of the P84 adsorbed by C45 leaves the Si@pitch 50:50 particles needing an additional 0.5 wt% of P84 to have the same electrode morphology observed with the Si@pitch 90:10 electrodes. Additionally, there is an increase in viscosity for the Si@pitch 50:50 electrode slurry when compared to the the Si@pitch 90:10 slurry (See Supporting Information and Figure S6). The increased viscosity makes for a thicker electrode with less porosity, which causes a tortuous path for electrolyte infiltration and lithium-ion mobility.[88] This data shows supports the interzonal hypothesis of binder adsorption to silicon based materials and conductive additives and that the balance of the ratio of Si:binder:carbon black is key in processing silicon based electrodes.

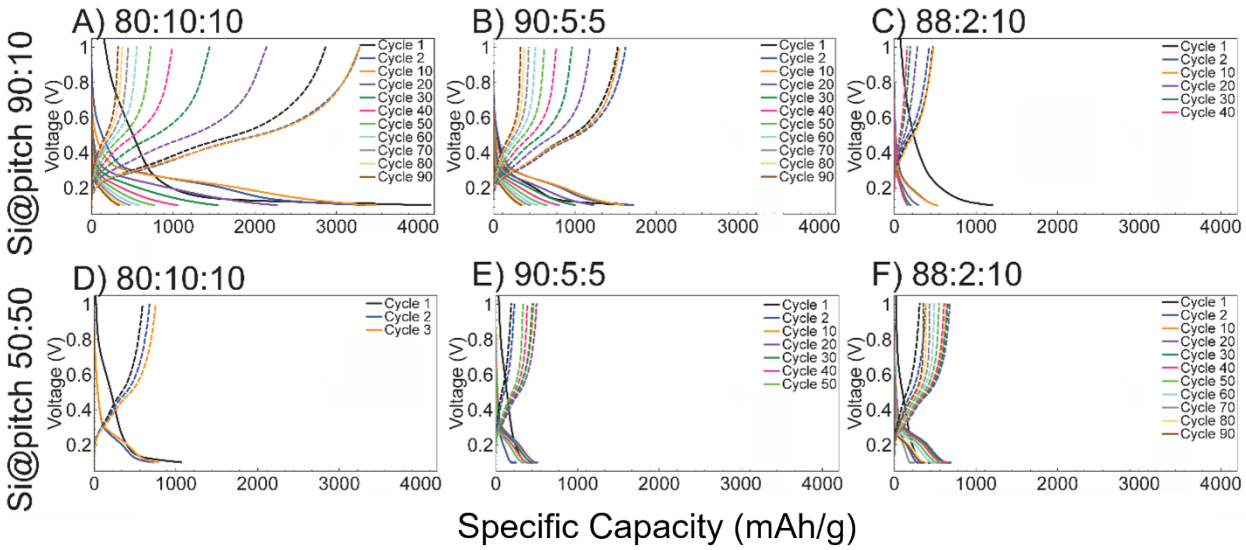

Figure 5: Voltage versus specific capacity profiles of electrode made with Si@pitch 90:10 (top) or Si@pitch 50:50 (bottom) active material where the Si@pitch:C45:P84 electrode formulation is 80:10:10 (A and D), 90:5:5 (B and E), or 88:2:10 (C and F).

Conclusions

Finding the interzonal region of binder adsorption on silicon active materials is vital to fabricating electrodes with optimized electrochemical properties. Binder adsorption can be controlled by adjusting the surface chemistry of silicon as shown through coating the silicon with pitch with various Si:pitch ratios. It is found that the balance between P84 adsorption to C45 and Si@pitch powders is key in electrode processing and is a factor that cannot be ignored any longer. Furthermore, rheo-USANS shows that there needs to be some heterogeneity in the electrode slurry, and, thus, the electrode itself, to provide structural stability and facilitate facile lithium-ion diffusion and electronic transport upon electrochemical cycling.

Acknowledgements

This research (MKBT, BLA, GMV) was supported by the U.S. Department of Energy's Vehicle Technologies Office under the Silicon Consortium Project, directed by Brian Cunningham, and managed by Anthony Burrell. A portion of this research used resources at the Spallation Neutron Source, a DOE Office of Science User Facility operated by Oak Ridge National Laboratory (MD and LH). The ultra-small angle scattering measurements were done using the USANS instrument at the Spallation Neutron Source. This work benefited from the use of the SasView application, originally developed under NSF award DMR-0520547. SasView contains code developed with funding from the European Union's Horizon 2020 research and innovation programme under the SINE2020 project, grant agreement no. 654000. The authors thank Paul Dodson and Bill Aronoff for their invaluable help with the GPC. This manuscript has been authored by UT-Battelle, LLC, under Contract DE-AC05-00OR22725 with the U.S. Department of Energy. The United States Government retains and the publisher, by accepting the article for publication, acknowledges that

the United States Government retains a nonexclusive, paid-up, irrevocable, worldwide license to publish or reproduce the published form of this manuscript, or allow other to do so, for United States Government purposes. The Department of Energy will provide public access to these results of federally sponsored research in accordance with the DOE Public Access Plan (http://energy.gov/downloads/doe-public-access-plan).

References

1. Bie, Y. T.; Yang, J.; Liu, X. L.; Wang, J. L.; Nuli, Y. N.; Lu, W., Polydopamine Wrapping Silicon Cross-linked with Polyacrylic Acid as High-performance Anode for Lithium-Ion Batteries. *ACS Appl. Mater. Interfaces* **2016,** *8* (5), 2899-2904.
2. Bie, Y. T.; Yang, J.; Lu, W.; Lei, Z. H.; Nuli, Y. N.; Wang, J. L., A Facile 3D Binding Approach for High Si Loading Anodes. *Electrochim. Acta* **2016,** *212*, 141-146.
3. Cao, P. F.; Yang, G.; Li, B. R.; Zhang, Y. M.; Zhao, S.; Zhang, S.; Erwin, A.; Zhang, Z. C.; Sokolov, A. P.; Nanda, J.; Saito, T., Rational Design of a Multifunctional Binder for High-capacity Silicon-Based Anodes. *ACS Energy Lett.* **2019,** *4* (5), 1171-1180.
4. Chartrel, T.; Ndour, M.; Bonnet, V.; Cavalaglio, S.; Aymard, L.; Dolhem, F.; Monconduit, L.; Bonnet, J. P., Revisiting and Improving the Preparation of Silicon-Based Electrodes for Lithium-Ion Batteries: Ball milling Impact on Poly(acrylic acid) Polymer Binders. *Mater. Chem. Front.* **2019,** *3* (5), 881-891.
5. Choi, J. W.; Aurbach, D., Promise and Reality of Post-Lithium-Ion Batteries with High Energy Densities. *Nat. Rev. Mater.* **2016,** *1* (4), 16013.
6. Ding, N.; Xu, J.; Yao, Y. X.; Wegner, G.; Lieberwirth, I.; Chen, C. H., Improvement of Cyclability of Si as Anode for Li-Ion Batteries. *J. Power Sources* **2009,** *192* (2), 644-651.
7. Erk, C.; Brezesinski, T.; Sommer, H.; Schneider, R.; Janek, J., Toward Silicon Anodes for Next-Generation Lithium Ion Batteries: A Comparative Performance Study of Various Polymer Binders and Silicon Nanopowders. *ACS Appl. Mater. Interfaces* **2013,** *5* (15), 7299-7307.
8. Gu, Y. Y.; Yang, S. M.; Zhu, G. B.; Yuan, Y. N.; Qu, Q. T.; Wang, Y.; Zheng, H. H., The Effects of Cross-Linking Cations on the Electrochemical Behavior of Silicon Anodes with Alginate Binder. *Electrochim. Acta* **2018,** *269*, 405-414.
9. He, J. R.; Zhang, L. Z., Polyvinyl Alcohol Grafted Poly (acrylic acid) as Water-Soluble Binder with Enhanced Adhesion Capability and Electrochemical Performances for Si Anode. *J. Alloys Compd.* **2018,** *763*, 228-240.
10. Huang, C. F.; Yu, L. B.; He, S. S.; Gan, L. H.; Liu, J.; Gong, Z. L.; Long, M. N., Influence of molecular structure of Carboxymethyl Cellulose on High Performance Silicon Anode in Lithium-Ion Batteries. *Int. J. Electrochem. Sci.* **2019,** *14* (5), 4799-4811.
11. Huang, L. H.; Chen, D.; Li, C. C.; Chang, Y. L.; Lee, J. T., Dispersion Homogeneity and Electrochemical Performance of Si Anodes with the Addition of Various Water-Based Binders. *J. Electrochem. Soc.* **2018,** *165* (10), A2239-A2246.
12. Hwang, C.; Joo, S.; Kang, N. R.; Lee, U.; Kim, T. H.; Jeon, Y.; Kim, J.; Kim, Y. J.; Kim, J. Y.; Kwak, S. K.; Song, H. K., Breathing Silicon Anodes for Durable High-Power Operations. *Sci. Rep.* **2015,** *5*, 14433.

13. Jeena, M. T.; Lee, J. I.; Kim, S. H.; Kim, C.; Kim, J. Y.; Park, S.; Ryu, J. H., Multifunctional Molecular Design as an Efficient Polymeric Binder for Silicon Anodes in Lithium-Ion Batteries. *ACS Appl. Mater. Interfaces* **2014,** *6* (20), 18001-18007.
14. Jeong, Y. K.; Kwon, T. W.; Lee, I.; Kim, T. S.; Coskun, A.; Choi, J. W., Millipede-Inspired Structural Design Principle for High Performance Polysaccharide Binders in Silicon Anodes. *Energy Environ. Sci.* **2015,** *8* (4), 1224-1230.
15. Kang, S.; Yang, K.; White, S. R.; Sottos, N. R., Silicon Composite Electrodes with Dynamic Ionic Bonding. *Adv. Energy Mat.* **2017,** *7* (17), 1700045.
16. Karkar, Z.; Guyomard, D.; Roue, L.; Lestriez, B., A Comparative Study of Polyacrylic Acid (PAA) and Carboxymethyl Cellulose (CMC) Binders for Si-based Electrodes. *Electrochim. Acta* **2017,** *258*, 453-466.
17. Komaba, S.; Shimomura, K.; Yabuuchi, N.; Ozeki, T.; Yui, H.; Konno, K., Study on Polymer Binders for High-Capacity SiO Negative Electrode of Li-Ion Batteries. *J. Phys. Chem. C* **2011,** *115* (27), 13487-13495.
18. Koo, B.; Kim, H.; Cho, Y.; Lee, K. T.; Choi, N. S.; Cho, J., A Highly Cross-Linked Polymeric Binder for High-Performance Silicon Negative Electrodes in Lithium Ion Batteries. *Angew. Chem. Int.* **2012,** *51* (35), 8762-8767.
19. Liu, J.; Zhang, Q.; Zhang, T.; Li, J. T.; Huang, L.; Sun, S. G., A Robust Ion-Conductive Biopolymer as a Binder for Si Anodes of Lithium-Ion Batteries. *Adv. Funct. Mater.* **2015,** *25* (23), 3599-3605.
20. Lopez, J.; Chen, Z.; Wang, C.; Andrews, S. C.; Cui, Y.; Bao, Z. N., The Effects of Cross-Linking in a Supramolecular Binder on Cycle Life in Silicon Microparticle Anodes. *ACS Appl. Mater. Interfaces* **2016,** *8* (3), 2318-2324.
21. Magasinski, A.; Zdyrko, B.; Kovalenko, I.; Hertzberg, B.; Burtovyy, R.; Huebner, C. F.; Fuller, T. F.; Luzinov, I.; Yushin, G., Toward Efficient Binders for Li-Ion Battery Si-based Anodes: Polyacrylic Acid. *ACS Appl. Mater. Interfaces* **2010,** *2* (11), 3004-3010.
22. Song, J. X.; Zhou, M. J.; Yi, R.; Xu, T.; Gordin, M. L.; Tang, D. H.; Yu, Z. X.; Regula, M.; Wang, D. H., Interpenetrated Gel Polymer Binder for High-Performance Silicon Anodes in Lithium-Ion Batteries. *Adv. Funct. Mater.* **2014,** *24* (37), 5904-5910.
23. Wei, L. M.; Chen, C. X.; Hou, Z. Y.; Wei, H., Poly(acrylic acid sodium) Grafted Carboxymethyl Cellulose as a High Performance Polymer Binder for Silicon Anode in Lithium Ion Batteries. *Sci. Rep.* **2016,** *6*, 19583.
24. Wu, Z. Y.; Deng, L.; Li, J. T.; Huang, Q. S.; Lu, Y. Q.; Liu, J.; Zhang, T.; Huang, L.; Sun, S. G., Multiple Hydrogel Alginate Binders for Si Anodes of Lithium-Ion Battery. *Electrochim. Acta* **2017,** *245*, 363-370.
25. Yoon, J.; Oh, D. X.; Jo, C.; Lee, J.; Hwang, D. S., Improvement of Desolvation and Resilience of Alginate Binders for Si-Based Anodes in a Lithium Ion Battery by Calcium-Mediated Cross-Linking. *Phys. Chem. Chem. Phys.* **2014,** *16* (46), 25628-25635.
26. Zhang, G. Z.; Yang, Y.; Chen, Y. H.; Huang, J.; Zhang, T.; Zeng, H. B.; Wang, C. Y.; Liu, G.; Deng, Y. H., A Quadruple-Hydrogen-Bonded Supramolecular Binder for High-Performance Silicon Anodes in Lithium-Ion Batteries. *Small* **2018,** *14* (29).
27. Zhang, L.; Zhang, L. Y.; Chai, L. L.; Xue, P.; Hao, W. W.; Zheng, H. H., A Coordinatively Cross-linked Polymeric Network as a Functional Binder for High-Performance Silicon Submicro-particle Anodes in Lithium-Ion Batteries. *J. Mater. Chem. A* **2014,** *2* (44), 19036-19045.
28. Zhu, G. B.; Gu, Y. Y.; Wang, Y.; Liu, G.; Battaglia, V. S.; Qu, Q. T.; Zheng, H. H., Suppressing the Dry Bed-Lake Fracture of Silicon Anode via Dispersant Modification in Electrode Processing. *Electrochim. Acta* **2019,** *319*, 682-689.

29. Zhu, L. L.; Du, F. H.; Zhuang, Y.; Dai, H.; Cao, H. S.; Adkins, J.; Zhou, Q.; Zheng, J. W., Effect of Crosslinking Binders on Li-Storage Behavior of Silicon Particles as Anodes for Lithium Ion Batteries. *J. Electroanal. Chem.* **2019,** *845*, 22-30.
30. Burdette-Trofimov, M. K.; Armstrong, B. L.; Heroux, L.; Doucet, M.; Sacci, R. L.; Veith, G. M., Structure and Dynamics of Small Polyimide Oligomers with Silicon as a Function of Aging. *Soft Matter* **2021,** *17* (33), 7729-7742.
31. Burdette-Trofimov, M. K.; Armstrong, B. L.; Murphy, R., P.; Heroux, L.; Doucet, M.; Rogers, A. M.; Veith, G. M., Probing Clustering Dynamics between Silicon and PAA or LiPAA Slurries under Processing Conditions *ACS Appl. Polym. Mater.* **2021,** *3* (5), 2447–2460.
32. Burdette-Trofimov, M. K.; Armstrong, B. L.; Murphy, R., P.; Heroux, L.; Doucet, M.; Trask, S. E.; Rogers, A. M.; Veith, G. M., Role of Low Molecular Weight Polymers on the Dynamics of Silicon Anodes During Casting. *ChemPhysChem* **2021,** *22* (11), 1049-1058.
33. Burdette-Trofimov, M. K.; Armstrong, B. L.; Rogers, A. M.; Heroux, L.; Doucet, M.; Yang, G.; Phillip, N. D.; Kidder, M. K.; Veith, G. M., Understanding Binder-Silicon Interactions During Slurry Processing. *J. Phys. Chem. C* **2020,** *124* (24), 13479-13494.
34. Burdette-Trofimov, M. K.; Armstrong, B. L.; Weker, J. N.; Rogers, A. M.; Yang, G.; Self, E. C.; Armstrong, R. R.; Nanda, J.; Veith, G. M., Direct Measure of Electrode Spatial Heterogeneity: Influence of Processing Conditions on Anode Architecture and Performance. *ACS Appl. Mater. Interfaces* **2020,** *12* (50), 55954-55970.
35. Zhang, Y. Z.; Pan, Y.; Chen, Y. J.; Lucht, B. L.; Bose, A., Towards Reducing Carbon Content in Silicon/Carbon Anodes for Lithium Ion Batteries. *Carbon* **2017,** *112*, 72-78.
36. Jeschull, F.; Trabesinger, S., Fast-Charge Limitations for Graphite Anodes with Si as Capacity-Enhancing Additive. *Batter. Supercaps* **2021,** *4* (1), 131-139.
37. Kierzek, K.; Machnikowski, J.; Beguin, F., Towards the Realistic Silicon/Carbon Composite for Li-Ion Secondary Battery Anode. *J. Appl. Electrochem.* **2015,** *45* (1), 1-10.
38. Shao, D.; Zhong, H. X.; Zhang, L. Z., Water-Soluble Conductive Composite Binder Containing PEDOT: PSS as Conduction Promoting Agent for Si Anode of Lithium-Ion Batteries. *ChemElectroChem* **2014,** *1* (10), 1679-1687.
39. Kim, B. G.; Shin, W. H.; Lim, S. Y.; Kong, B. S.; Choi, J. W., A Carbon Nanotubes-Silicon Nanoparticles Network for High Performance Lithium Rechargeable Battery Anodes. *J. Electrochem. Sci. Technol.* **2012,** *3* (3), 116-122.
40. Li, P.; Hwang, J. Y.; Sun, Y. K., Nano/Microstructured Silicon-Graphite Composite Anode for High-Energy-Density Li-Ion Battery. *ACS Nano* **2019,** *13* (2), 2624-2633.
41. Sarkar, A.; Daniels-Race, T., Electrophoretic Deposition of Carbon Nanotubes on 3-Amino-Propyl-Triethoxysilane (APTES) Surface Functionalized Silicon Substrates. *Nanomaterials* **2013,** *3* (2), 272-288.
42. Wang, W.; Epur, R.; Kumta, P. N., Vertically Aligned Silicon/Carbon Nanotube (VASCNT) Arrays: Hierarchical Anodes for Lithium-Ion Battery. *Electrochem. commun.* **2011,** *13* (5), 429-432.
43. Zhou, Z. B.; Xu, Y. H.; Hojamberdiev, M.; Liu, W. G.; Wang, J. A., Enhanced Cycling Performance of Silicon/Disordered Carbon/Carbon Nanotubes Composite for Lithium Ion Batteries. *J. Alloys Compd.* **2010,** *507* (1), 309-311.
44. Choi, S. H.; Nam, G.; Chae, S.; Kim, D.; Kim, N.; Kim, W. S.; Ma, J.; Sung, J.; Han, S. M.; Ko, M.; Lee, H. W.; Cho, J., Robust Pitch on Silicon Nanolayer-Embedded Graphite for Suppressing Undesirable Volume Expansion. *Adv. Energy Mater.* **2019,** *9* (4).
45. Chew, S. Y.; Guo, Z. P.; Wang, J. Z.; Chen, J.; Munroe, P.; Ng, S. H.; Zhao, L.; Liu, H. K., Novel Nano-Silicon/Polypyrrole Composites for Lithium Storage. *Electrochem. commun.* **2007,** *9* (5), 941-946.
46. Su, L. W.; Zhou, Z.; Ren, M. M., Core Double-Shell Si@SiO_2@C Nanocomposites as Anode Materials for Li-Ion Batteries. *Chem. Commun.* **2010,** *46* (15), 2590-2592.

47. Wang, D. S.; Gao, M. X.; Pan, H. G.; Wang, J. H.; Liu, Y. F., High Performance Amorphous-Si@SiO_x/C Composite Anode Materials for Li-Ion Batteries Derived from Ball-Milling and *in situ* Carbonization. *J. Power Sources* **2014,** *256*, 190-199.
48. Yoshio, M.; Wang, H. Y.; Fukuda, K.; Umeno, T.; Dimov, N.; Ogumi, Z., Carbon-Coated Si as a Lithium-Ion Battery Anode Material. *J. Electrochem. Soc.* **2002,** *149* (12), A1598-A1603.
49. Arie, A. A.; Chang, W.; Lee, J. K., Effect of Fullerene Coating on Silicon Thin Film Anodes for Lithium Rechargeable Batteries. *J. Solid State Electrochem.* **2010,** *14* (1), 51-56.
50. Kim, Y. M.; Ahn, J.; Yu, S. H.; Chung, D. Y.; Lee, K. J.; Lee, J. K.; Sung, Y. E., Titanium Silicide Coated Porous Silicon Nanospheres as Anode Materials for Lithium Ion Batteries. *Electrochim. Acta* **2015,** *151*, 256-262.
51. Nguyen, S. H.; Lim, J. C.; Lee, J. K., Improving the Performance of Silicon Anode in Lithium-Ion Batteries by Cu_2O Coating Layer. *J. Appl. Electrochem.* **2014,** *44* (3), 353-360.
52. Sim, S.; Oh, P.; Park, S.; Cho, J., Critical Thickness of SiO_2 Coating Layer on Core@Shell Bulk@Nanowire Si Anode Materials for Li-Ion Batteries. *Adv. Mater.* **2013,** *25* (32), 4498-4503.
53. Yu, Y.; Gu, L.; Zhu, C. B.; Tsukimoto, S.; van Aken, P. A.; Maier, J., Reversible Storage of Lithium in Silver-Coated Three-Dimensional Macroporous Silicon. *Adv. Mater.* **2010,** *22* (20), 2247-2250.
54. Escamilla-Perez, A. M.; Roland, A.; Giraud, S.; Guiraud, C.; Virieux, H.; Demoulin, K.; Oudart, Y.; Louvain, N.; Monconduit, L., Pitch-Based Carbon/Nano-Silicon Composite, an Efficient Anode for Li-Ion Batteries. *RSC Adv.* **2019,** *9* (19), 10546-10553.
55. Kumar, S. K.; Ghosh, S.; Malladi, S. K.; Nanda, J.; Martha, S. K., Nanostructured Silicon-Carbon 3D Electrode Architectures for High-Performance Lithium-Ion Batteries. *ACS Omega* **2018,** *3* (8), 9598-9606.
56. Lu, Z. W.; Zhang, L. Q.; Liu, X. J., Microstructure and Electrochemical Performance of Si-SiO_2-C Composites as the Negative Material for Li-Ion Batteries. *J. Power Sources* **2010,** *195* (13), 4304-4307.
57. Ma, C. L.; Wang, Z. R.; Zhao, Y.; Li, Y.; Shi, J., A Novel Raspberry-Like Yolk-Shell Structured Si/C Micro/Nano-Spheres as High-Performance Anode Materials for Lithium-Ion Batteries. *J. Alloys Compd.* **2020,** *844*.
58. Park, G. D.; Choi, J. H.; Jung, D. S.; Park, J. S.; Kang, Y. C., Three-Dimensional Porous Pitch-Derived Carbon Coated Si Nanoparticles-CNT Composite Microsphere with Superior Electrochemical Performance for Lithium Ion Batteries. *J. Alloys Compd.* **2020,** *821*.
59. Qu, F. M.; She, G. W.; Wang, J. T.; Qi, X. P.; Li, S. Y.; Zhang, S. Y.; Mu, L. X.; Shi, W. S., Coating Nanoparticle-Assembled Si Microspheres with Carbon for Anode Material in Lithium-Ion Battery. *J. Phys. Chem. Solids* **2019,** *124*, 312-317.
60. Tao, Y.; Tian, Y.; An, Y. L.; Wei, C. L.; Li, Y.; Zhang, Q. K.; Feng, J. K., Green and Facile Fabrication of Nanoporous Silicon@Carbon from Commercial Alloy with High Graphitization Degree for High-Energy Lithium-Ion Batteries. *SM&T* **2021,** *27*.
61. Uono, H.; Kim, B. C.; Fuse, T.; Ue, M.; Yamaki, J. I., Optimized Structure of Silicon/Carbon/Graphite Composites as an Anode Material for Li-Ion Batteries. *J. Electrochem. Soc.* **2006,** *153* (9), A1708-A1713.
62. Mikhailets, N. R.; Sinitsin, S. A.; Danilov, E. A., Thermal Polycondensation Process and Petroleum Pitch Production. *Chem. Technol. Fuels Oils.* **2021,** *57* (2), 216-223.
63. Mukhamedzyanova, A. A.; Khaibullin, A. A.; Telyashev, E. G.; Gimaev, R. N., Production of Petroleum Pitch from Oil Refinery Residues. *Chem. Technol. Fuels Oils.* **2011,** *47* (2), 90-96.
64. Srivastava, M.; Gupta, S.; Thapliyal, M.; Aloopwan, M. K. S.; Kaushik, R. S.; Singh, I. D.; Anwar, M.; Garg, M. O., Upgrading Low Value Refinery Streams into Electrode Grade Petroleum Pitch. *Pet. Sci. Technol.* **2003,** *21* (5-6), 699-707.

65. Chen, C. Y.; Liang, A. H.; Huang, C. L.; Hsu, T. H.; Li, Y. Y., The Pitch-Based Silicon-Carbon Composites Fabricated by Electrospraying Technique as the Anode Material of Lithium Ion Battery. *J. Alloys Compd.* **2020,** *844*.
66. Xing, W. B.; Wilson, A. M.; Zank, G.; Dahn, J. R., Pyrolysed Pitch-Polysilane Blends for Use as Anode Materials in Lithium Ion Batteries. *Solid State Ion.* **1997,** *93* (3-4), 239-244.
67. Sinha, P.; Datar, A.; Jeong, C.; Deng, X. P.; Chung, Y. G.; Lin, L. C., Surface Area Determination of Porous Materials Using the Brunauer-Emmett-Teller (BET) Method: Limitations and Improvements. *J. Phys. Chem. C* **2019,** *123* (33), 20195-20209.
68. Brandl, G.; Georgii, R.; Haussler, W.; Muhlbauer, S.; Boni, P., Large Scales-Long Times: Adding High Energy Resolution to SANS. *Nucl. Instrum. Methods Phys. Res.* **2011,** *654* (1), 394-398.
69. Carpenter, J. M.; Agamalian, M.; Iop, Aiming for the Theoretical Limit of Sensitivity of Bonse-Hart USANS Instruments. In *International Conference on Neutron Scattering 2009*, 2010; Vol. 251.
70. Agamalian, M.; Heroux, L.; Littrell, K. C.; Carpenter, J. M.; Iop, Progress on the Time-of-Flight Ultra Small Angle Neutron Scattering Instrument at SNS. In *22nd Meeting of the International Collaboration on Advanced Neutron Sources*, 2018; Vol. 1021.
71. Arnold, O.; Bilheux, J. C.; Borreguero, J. M.; Buts, A.; Campbell, S. I.; Chapon, L.; Doucet, M.; Draper, N.; Leal, R. F.; Gigg, M. A.; Lynch, V. E.; Markvardsen, A.; Mikkelson, D. J.; Mikkelson, R. L.; Miller, R.; Palmen, K.; Parker, P.; Passos, G.; Perring, T. G.; Peterson, P. F.; Ren, S.; Reuter, M. A.; Savici, A. T.; Taylor, J. W.; Taylor, R. J.; Tolchenoy, R.; Zhou, W.; Zikoysky, J., Mantid-Data Analysis and Visualization Package for Neutron Scattering and *μSR* experiments. *Nucl. Instrum. Methods Phys. Res.* **2014,** *764*, 156-166.
72. Doucet, M.; Cho, J. H.; Alina, G.; Bakker, J.; Bouwman, W.; Butler, P.; Campbell, K.; Cooper-Benun, T.; Durniak, C.; Forster, L.; Gonzales, M.; Heenan, R.; Jackson, A.; King, S.; Kienzle, P.; Krzywon, J.; Nielsen, T.; O'Driscoll, L.; Potrzebowski, W.; Ferraz Leal, R.; Rozycko, P.; Snow, T.; Washington, A. *SasView*, 5.0; Zenodo: 2019.
73. Chow, A. W.; Sinton, S. W.; Iwamiya, J. H.; Stephens, T. S., Shear-Induced Particle Migration in Couette and Parallel-Plate Viscometers-NMR Imaging and Stress Measurements. *Phys. Fluids* **1994,** *6* (8), 2561-2576.
74. Dejeu, J.; Foissy, A.; Membrey, F.; Balastre, M.; Bordes, B., Laser Reflectometry: Examination of the Influence of Some Assumptions and Approximations to Calculate the Adsorption from the Reflectometric Signal. *Colloid Surf. A-Physicochem Eng. Asp.* **2007,** *310* (1-3), 78-85.
75. Kampf, N.; Raviv, U.; Klein, J., Normal and Shear Forces Between Adsorbed and Gelled Layers of Chitosan, a Naturally Occurring Cationic Polyelectrolyte. *Macromolecules* **2004,** *37* (3), 1134-1142.
76. Zeng, J. R.; Cheng, C. C.; Lee, A. W.; Wei, P. L.; Chen, J. K., Visualization Platform of One-Dimensional Gratings of Tethered Polyvinyltetrazole Brushes on Silicon Surfaces for Sensing of Cr(III). *Microchim. Acta* **2017,** *184* (8), 2723-2730.
77. Principles underlying the dyeing process. In *Modelling, Simulation and Control of the Dyeing Process*, Shamey, R.; Zhao, X., Eds. Elsevier Ltd: 2014; pp 31-53.
78. Hammouda, B., Solvation Characteristics of a Model Water-Soluble Polymer. *J. Polym. Sci. Pol. Phys.* **2006,** *44* (22), 3195-3199.
79. Hammouda, B.; Ho, D. L.; Kline, S., Insight into Clustering in Poly(ethylene oxide) Solutions. *Macromolecules* **2004,** *37* (18), 6932-6937.
80. Konduri, M. K. R.; Fatehi, P., Designing Anionic Lignin Based Dispersant for Kaolin Suspensions. *Colloid Surf. A-Physicochem. Eng. Asp.* **2018,** *538*, 639-650.
81. Roby, S. H.; Yamaguchi, E. S.; Francisco, M. M.; Ruelas, S. G., Antiwear Film Formation by ZnDTP, Detergent, and Dispersant Components of Passenger Car Motor Oils - Part II: Effects of Low-Molecular-Weight Dispersant on Film Formation. *Tribol. Trans.* **2004,** *47* (4), 517-521.

82. Sato, K.; Kondo, S.; Tsukada, M.; Ishigaki, T.; Kamiya, H., Influence of Solid Fraction on the Optimum Molecular Weight of Polymer Dispersants in Aqueous TiO_2 Nanoparticle Suspensions. *J. Am. Ceram. Soc.* **2007,** *90* (11), 3401-3406.
83. Yang, D. J.; Li, H. J.; Qin, Y. L.; Zhong, R. S.; Bai, M. X.; Qiu, X. Q., Structure and Properties of Sodium Lignosulfonate with Different Molecular Weight Used as Dye Dispersant. *J. Dispers. Sci. Technol.* **2015,** *36* (4), 532-539.
84. Hall, L. M.; Jayaraman, A.; Schweizer, K. S., Molecular Theories of Polymer Nanocomposites. *Curr. Opin. Solid State Mater. Sci.* **2010,** *14* (2), 38-48.
85. Wang, Z.; Du, L. Z., Stabilization of a Novel Mixed Solution Precursor used for Preparing YSZ Abradable Sealing Coatings. *Colloids Surf. A Physicochem. Eng. Asp.* **2019,** *562*, 354-360.
86. Browning, K. L.; Sacci, R. L.; Doucet, M.; Browning, J. F.; Kim, J. R.; Veith, G. M., The Study of the Binder Poly(acrylic acid) and its Role in Concomitant Solid-Electrolyte Interphase Formation on Si Anodes. *ACS Appl. Mater. Interfaces* **2020,** *12* (8), 10018-10030.
87. Mezger, T. G., *Applied Rheology*. 4 ed.; Anton Paar GmbH: Graz, Austria, 2017; p 192.
88. Gao, S. L.; Sun, F. Y.; Brady, A.; Pan, Y. Y.; Erwin, A.; Yang, D. D.; Tsukruk, V.; Stack, A. G.; Saito, T.; Yang, H. B.; Cao, P. F., Ultra-Efficient Polymer Binder for Silicon Anode in High-Capacity Lithium-Ion Batteries. *Nano Energy* **2020,** *73*.